Thermocapillary Flow in an Annular Two-Layer Liquid System

Haiqiong Xie[1], Zhong Zeng[1,2,*], Liangqi Zhang[1], Yuui Yokota[2], Yoshiyuki Kawazoe[2] and Akira Yoshikawa[2]

[1]*Department of Engineering Mechanics, Chongqing University, Chongqing 400044, P. R. China*

[2]*Institute for Materials Research, Tohoku University, Sendai 980-8577, Japan*

[3]*New Industry Creation Hatchery Center, Tohoku University, Sendai 980-8579, Japan*

Abstract: By means of a hybrid lattice Boltzmann method, thermocapillary flow, driven by the surface tension owing to a horizontal temperature gradient along the interface in immiscible two-layer liquid system, is simulated numerically. The dynamic behavior of the interface is captured by using phase-field theory. The dependence of flow and interface deformation on the density ratio, Capillary number and aspect ratio, is investigated.

Keywords: Thermocapillary flow, Interface deformation, Lattice Boltzmann method.

1. INTRODUCTION

Thermocapillary flow, a surface tension-driven flow, has received considerable attention in numerous engineering applications, particularly for the liquid encapsulation crystal (LEC) growth technique under microgravity [1-4]. It is important to understand the behavior of thermocapillary flow and the dynamical deformation of the interface in two liquid layers to achieve the significant advantages of the LEC technique.

Liu *et al*. [5] simulated a flow in a two layers system subject to a horizontal temperature gradient, and assumed a flat interface between two immiscible fluids. They applied liquid encapsulation to suppress thermocapillary flow in the melt under microgravity conditions. Gupta *et al.* [6] adopted the finite difference method with a staggered grid and domain mapping technique to solve the temperature field and flow field, an effective single-layer model, approximating the flow within the encapsulated layer, was developed. Koster *et al*. [7] pointed out that, from the experimental view, a more detailed investigation of thermocapillary flow in multilayered fluid system is needed to account for finite interface deformations.

In the present paper, thermocapillary flow with the deformable interface in an annular two-layer liquid system is simulated with an axisymmetric hybrid model, coupling finite difference method (FDM) with a multiple relaxation-time (MRT) lattice Boltzmann method (LBM). The phase-field theory is introduced to capture the deformation of the liquid-liquid interface.

*Address correspondence to this author at the Department of Engineering Mechanics, Chongqing University, Chongqing 400044, P. R. China;
Tel: +86 13638333680; Fax: +86 23 65111067; E-mail: zzeng@cqu.edu.cn

2. NUMERICAL METHOD

2.1. Axisymmetric LBM for Fluids

In LBM, $f_\alpha(x, t)$ is defined as a particle distribution function at position x(r, z), time t with velocity e_α. The evolution equation for $f_\alpha(x, t)$ with a single relaxation time collision model is:

$$f_\alpha(\mathbf{x}+\mathbf{e}_\alpha\delta_t, t+\delta_t) - f_\alpha(\mathbf{x},t) = -\frac{1}{\tau}[f_\alpha(\mathbf{x},t) - f_\alpha^{eq}(\mathbf{x},t)] \quad (1)$$

where $f_\alpha^{eq}(\mathbf{x},t)$ is the equilibrium distribution function, and τ, the single relaxation time, is related to the kinematic viscosity v. In a two dimensional nine-velocity (D2Q9) model, the $\mathbf{e}_\alpha$ is:

$$\mathbf{e}_\alpha = \begin{cases} (0,0), & \alpha = 0 \\ \left(\cos\left[(\alpha-1)\pi/2\right], \sin\left[(\alpha-1)\pi/2\right]\right)c, & \alpha = 1-4 \\ \left(\cos\left[(2\alpha-9)\pi/4\right], \sin\left[(2\alpha-9)\pi/4\right]\right)\sqrt{2}c, & \alpha = 5-8, \end{cases} \quad (2)$$

where $c=\delta_x/\delta_t$ is the lattice velocity. The equilibrium distribution function $f_\alpha^{eq}(\mathbf{x},t)$ is:

$$f_\alpha^{eq} = \omega_\alpha\left[p + \rho c_s^2\left(\frac{\mathbf{e}_\alpha\cdot\mathbf{u}}{c_s^2} + \frac{(\mathbf{e}_\alpha\cdot\mathbf{u})^2}{2c_s^4} - \frac{\mathbf{u}^2}{2c_s^2}\right)\right], \quad (3)$$

where $c_s^2 = c/3$, and the weight coefficients are:

$$\omega_\alpha = \begin{cases} 4/9, & \alpha = 0 \\ 1/9, & \alpha = 1,2,3,4 \\ 1/36, & \alpha = 5,6,7,8 \end{cases}. \quad (4)$$

Next, the external force is added directly in the right hand side of the evolution equation (1):

E-ISSN: 2409-5826/16

$$f_\alpha(\mathbf{x}+\mathbf{e}_\alpha\delta_t, t+\delta_t) - f_\alpha(\mathbf{x},t) = -\frac{1}{\tau}[f_\alpha(\mathbf{x},t) - f_\alpha^{eq}(\mathbf{x},t)] + \left(1-\frac{1}{\tau}\right)\left\{(\mathbf{e}_\alpha - \mathbf{u})\cdot\left[\nabla\rho c_s^2\left(\Gamma_\alpha - \Gamma_\alpha(0)\right)\right] + \left(\mathbf{F_s} + \mathbf{F}_{1,axis}\right)\Gamma_\alpha - \omega_\alpha F_{0,axis}\right\} \quad (5)$$

where $F_{0,axis}$ is a source term to account for the axisymmetric effect in the continuity equation, and $\mathbf{F}_{1,axis}$ is the parts to mimic the axisymmetric contribution for the momentum equation:

$$F_{0,axis} = c_s^2\frac{\rho u_r}{r}\quad \mathbf{F}_{1,axis} = \left(F_{r,axis}, F_{z,axis}\right) = \left(\rho\frac{\nu}{r}\frac{\partial u_r}{\partial r} + \rho\frac{\nu}{r}\frac{\partial u_r}{\partial r} - \rho\frac{u_r u_r}{r} - 2\rho\frac{\nu u_r}{r^2}, \rho\frac{\nu}{r}\frac{\partial u_z}{\partial r} + \rho\frac{\nu}{r}\frac{\partial u_r}{\partial z} - \rho\frac{u_r u_z}{r}\right) \quad (6)$$

Γ_α is defined as,

$$\Gamma_\alpha = \omega_\alpha\left(1 + \frac{\mathbf{e}_\alpha\cdot\mathbf{u}}{c_s^2} + \frac{(\mathbf{e}_\alpha\cdot\mathbf{u})^2}{2c_s^4} - \frac{\mathbf{u}^2}{2c_s^2}\right). \quad (7)$$

Because of the drawback of the instability at low viscosity values in the single relaxation time LBM model, a multiple-relaxation-time (MRT) collision model is adopted. The collision step in the right hand side of the Eq.(5) is implemented in the moment space:

$$\Omega = -\mathbf{M}^{-1}\mathbf{S}[\mathbf{m}(\mathbf{x},t) - \mathbf{m}^{eq}(\mathbf{x},t)], \quad (8)$$

where **m** and $\mathbf{m}^{eq}$ are moments and their corresponding equilibriums, and **S** is a diagonal matrix:

$$\mathbf{S} = \mathrm{diag}\left(s_0, s_1, s_2, s_3, s_4, s_5, s_6, s_7, s_8\right), \quad (9)$$

whose components represent the inverse of the relaxation time for the transformed distribution function $\mathbf{m}$ relaxing to the equilibrium distribution function $\mathbf{m}^{eq}$ in moment space. The transformation between the velocity space and moment space is achieved by the matrix **M**, which serves as a transformation matrix, and maps the distribution functions $\mathbf{f}(\mathbf{x}, t)$ to their moments:

$$\mathbf{m} = \mathbf{M}\mathbf{f}\quad \mathbf{f} = \mathbf{M}^{-1}\mathbf{m}. \quad (10)$$

The transformation matrix **M** is constructed via the Gram-Schmidt orthogonalization procedure from some polynomials of the components of the discrete velocities. The equilibrium moments can be obtained from $\mathbf{m}^{eq} = \mathbf{M}\mathbf{f}^{eq}$.

In the numerical implementation of this axisymmetric MRT LBM model, the collision step is conducted in the moment space, whereas the streaming step is still operated in the velocity space. The hydrodynamic fields, such as the dynamic pressure p and the velocity **u**, are derived from the appropriate moments of the distribution function as:

$$p = \sum_\alpha f_\alpha + \frac{\delta t}{2}\left(\mathbf{u}\cdot\nabla\rho c_s^2 - c_s^2\frac{\rho u_r}{r}\right),\quad \mathbf{u} = \frac{1}{\rho}\left(\frac{1}{c_s^2}\sum_\alpha \mathbf{e}_\alpha f_\alpha + \frac{1}{2}\mathbf{F}_s + \frac{1}{2}\mathbf{F}_{1,axis}\right) \quad (11)$$

2.2. Phase-Field Theory

In the phase-field model, a sharp fluid interface is replaced by a thin but nonzero thickness transition region where the interfacial forces are smoothly distributed and an order parameter φ is used to distinguish the different phases: φ=1 represents the phase one and φ=-1 for the other. The time dependent interface profile and the evolution of order parameter φ can be described by the Cahn-Hilliard equation [8, 9]

$$\frac{\partial\varphi}{\partial t} + \mathbf{u}\cdot\nabla\varphi = \nabla\left(M\nabla\mu_\varphi\right), \quad (12)$$

M is a diffusion parameter named as mobility or Onsager coefficient and μ_φ is the chemical potential which is related to the free energy of the system [8]:

$$\Upsilon(\varphi) = \int_V\left[\psi(\varphi) + \frac{\varepsilon^2}{2}|\nabla\varphi|^2\right]dV \quad (13)$$

where V is the region of space occupied by the system. The term $\psi(\varphi)$ is the bulk energy density and takes the form:

$$\psi(\varphi) = \frac{1}{4}\left(\varphi^2 - 1\right)^2. \quad (14)$$

The chemical potential μ_φ is defined as the variation derivative of the free-energy function with respect to the order parameter:

$$\mu_\varphi = \frac{\delta\Upsilon}{\delta\varphi} = \frac{\partial\psi}{\partial\varphi} - \varepsilon^2\nabla^2\varphi = \varphi^3 - \varphi - \varepsilon^2\nabla^2\varphi, \quad (15)$$

where the Laplacian of φ for axisymmetric flows in cylindrical coordinates is:

$$\nabla^2\varphi = \frac{\partial^2\varphi}{\partial r^2} + \frac{1}{r}\frac{\partial\varphi}{\partial r} + \frac{\partial^2\varphi}{\partial z^2}. \quad (16)$$

2.2.1 Variable Properties of the Fluids

In terms of two-phase flow, each phase is assumed as incompressible flow, and the fluid properties are

taken as constant in each phase. The reconstruction of the fluid properties $b(\varphi, t)$ at time t in the whole two-layer liquid system is achieved through the order parameter;

$$b(\varphi,t) = b_2 + \frac{\varphi-\varphi_2}{\varphi_1-\varphi_2}(b_2 - b_1) \tag{17}$$

where b represents the fluid density ρ, thermal conductivity κ, kinematic viscosity v and heat capacity c_p. In the following presentation, subscripts '1' and '2' denote the variable associated with the upper layer liquid and the lower layer liquid, respectively.

2.2.2 Surface Tension Model

The surface tension is a result of unbalanced forces exerted to the molecules near the interface of the two phases. In the numerical simulation, the continuum surface force model (CSF) [10] has been widely used and the surface tension is reformulated as a volume force in the momentum equation which only acts in the vicinity of the interface. The expression for the surface tension $\mathbf{F}_s$ is given by;

$$\mathbf{F}_s = (-\sigma k\mathbf{n} + \nabla_s\sigma)\delta_s \tag{18}$$

where the first term in the right side is the normal surface tension and the second term expresses the tangential force, which appears due to non-uniform surface tension. $\nabla_s = (\mathbf{I}-\mathbf{nn})\cdot\nabla$ is the surface gradient operator and δ_s is the Dirac function [8]. The interface normal **n** and curvature k can be obtained from the order parameter;

$$\mathbf{n} = \frac{\nabla\varphi}{|\nabla\varphi|}, \qquad k = \nabla\cdot\mathbf{n} \tag{19}$$

The surface tension σ is considered to be linearly dependent on temperature as;

$$\sigma(T) = \sigma_0 + \sigma_T(T - T_0) \tag{20}$$

where σ_0 is the surface tension coefficient at a reference temperature T_0 and σ_T is a negative constant for most of fluids.

2.3 Temperature Equation

The governing equation of the temperature field can be formulated as;

$$\rho c_p\left(\frac{\partial T}{\partial t} + \mathbf{u}\cdot\nabla T\right) = \nabla(\kappa\nabla T). \tag{21}$$

In the present hybrid model, the equations (11) and (20) are discretized on the same grid as the evolution Eq.(4) by a finite difference method and they are updated at the same time. The two equations can be rewritten in the following manner;

$$\frac{\partial\theta}{\partial t} = \mathbb{R}(\theta) = -\mathbf{u}\cdot\nabla\theta + \frac{1}{\vartheta}\left[\nabla\xi\cdot\nabla\theta + \xi\left(\frac{\partial^2\theta}{\partial r^2} + \frac{1}{r}\frac{\partial\theta}{\partial r} + \frac{\partial^2\theta}{\partial z^2}\right)\right] \tag{22}$$

where θ can be the order parameter or temperature, ϑ equal to ρc_p in the temperature equation, and ξ represents the diffusion parameter. The right hand side in Eq.(21) contains all the spatial derivatives, and the time stepping, in the left side, an explicit fourth-order Runge–Kutta scheme is employed.

3. NUMERICAL RESULTS

As shown in Figure **1**, the top and bottom rigid walls of the cavity are insulated, whereas the inner and outer walls are maintained at constant temperatures: the inner wall with a low temperature T_c and the outer wall with a high temperature T_h. Here, r_i is inner radius, H is the total thickness and L is the length of the annular cavity, respectively. Each liquid layer is characterized by its thickness H_i, density ρ_i, thermal conductivity κ_i, and kinematic viscosity v_i (the subscript i=1, 2). The important non-dimensional parameters are the Reynolds (Re), Marangoni (Ma), and Capillary number (Ca) as;

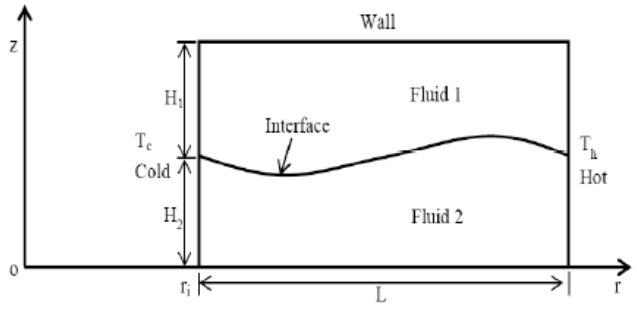

Figure 1: Schematic of the two liquid layers annular cavity with the outer heated wall and inner cooled wall.

$$\mathrm{Re} = \frac{LU}{\nu_2}, \qquad \mathrm{Ma} = \frac{\rho_2 c_{p2} LU}{\kappa_2}, \qquad \mathrm{Ca} = \frac{\rho_2\nu_2 U}{\sigma_0} \tag{23}$$

where the subscript 2 represents the lower liquid layer, and U is the reference velocity defined by the balance of tangential stress at the interface [1];

$$U = -\frac{\sigma_T\Delta T}{\rho_2\nu_2} \tag{24}$$

where ΔT ($\Delta T = T_h - T_c$) is temperature difference imposed across the annular cavity. The Prandtl number

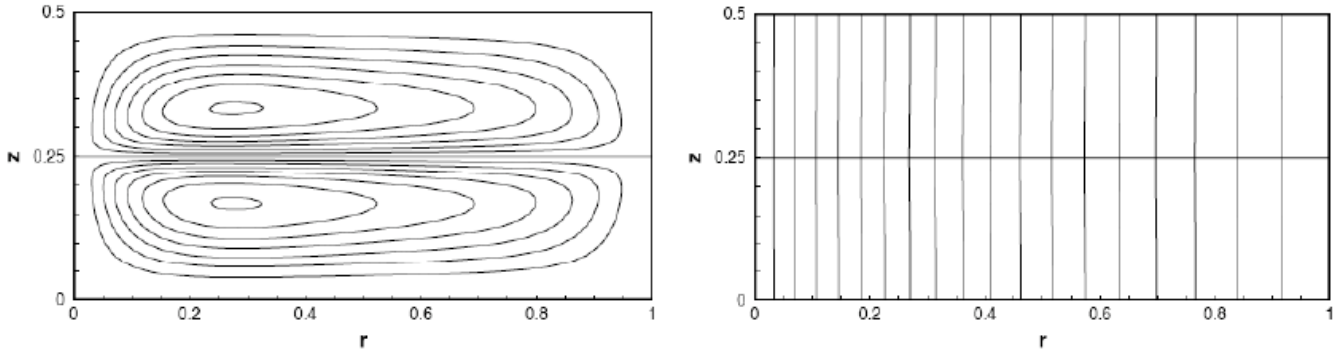

Figure 2: The streamlines (**a**) and isotherms (**b**) for thermocapillary convection with Re=10.

(Pr) is defined as Pr=v/κ. Non-slip (bounce-back) boundary conditions are employed at all the solid walls. The relaxation rates s_7 and s_8 are determined by the kinematic viscosity $s_7=s_8=1.0/(3.0v+0.5)$.

The streamlines and isotherms of the thermocapillary flow is exhibited in Figure **2** for Re=10 with $\rho_1=\rho_2=1.0$, $c_{p1}=c_{p2}=1.0$, $\sigma_T=-1\times10^{-4}$, $\sigma_0=2.5\times10^{-3}$, Pr=1.0, and ΔT=20. The computa-tional domain is H×L=100×200 and r_i=0.5L lattice units. For Re=10, the convection has little influence on the temperature field, and the isotherms remain nearly vertical as in Figure **2**. The flow features of the two liquid layers are thermocapillary convection cells, counter-rotating, and each layer is occupied by one. In addition, there is no deformation of interface shape because the thermocapillary flows in upper and lower liquid layers are fully symmetric owing to the same physical properties and geometrical conditions.

The comparison of radial velocity profile with different density ratios is demonstrated in Figure **3**. The

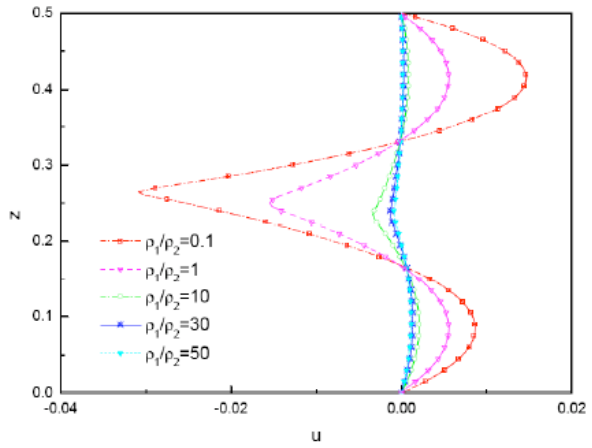

Figure 3: The radial velocity profiles along the z-axis at r=0.5L with different density ratios: ρ1/ρ2=0.1, ρ1/ρ2=1.0, ρ1/ρ2=10, ρ1/ρ2=30, and ρ1/ρ2=50.

different ratios are achieved by varying the density of the upper layer liquid while the lower is fixed at 1.0. Clearly, a heavier upper liquid layer (ρ_1/ρ_2=10, 30, and 50) leads to a reduction of the velocities in both layers, while for ρ_1/ρ_2=0.1, the velocities in both layers is increased apparently. In fact, a larger density ratio, represents a larger dynamic viscosity (the kinematic viscosities between the two layers keeping equal) for upper layer liquid because of the fixed density at lower liquid layer, and it takes more energy to overcome a larger viscosity resistance for thermocapillary flow, and therefore, the flow intensity decreases with increasing ρ_1/ρ_2. Figure **3** also shows that the magnitude of the velocities in both layers is not equal when the densities between the upper and lower layer are different, and the interface deformation with different density ratios is shown in Figure **4**.

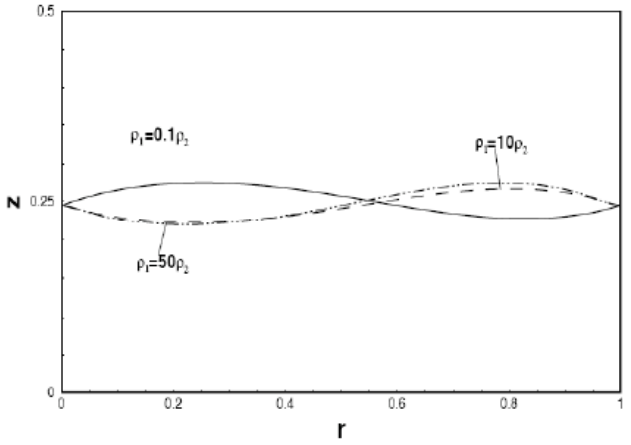

Figure 4: The interface deformation with different density ratios: ρ1/ρ2=0.1, ρ1/ρ2=10, and ρ1/ρ2=50.

Figure **5** illustrates the influence of different aspect ratios on the radial velocity profile. The different aspect ratios are achieved by varying the H_1 while the lower is fixed at H_2=75 lattice units. For $H_1/L<0.375$ ($H_1<H_2$), the velocity in the upper layer is reduced which resulting

the flow intensity in the lower layer is retarded through the viscous coupling at the interface, while for $H_1/L>0.375$ ($H_1>H_2$), in the upper layer, the magnitude of velocity is relatively unaffected by the aspect ratios which also reflecting in the lower layer. The results indicate that the retarding effect of the top rigid wall to the flow is more obvious with a small H_1. Figure **6** indicates the effect of the aspect ratios on the interface deformation.

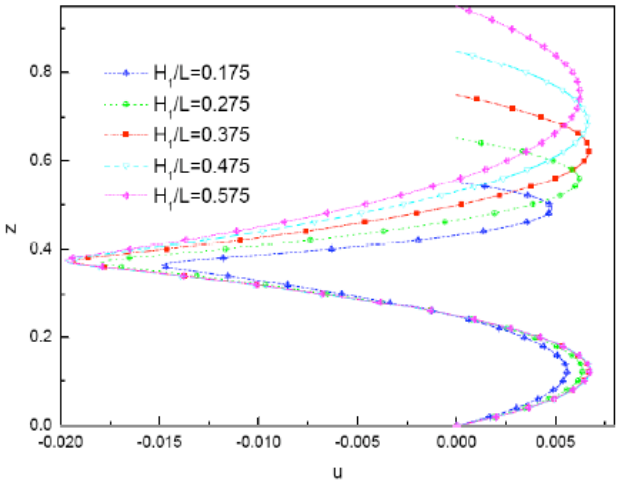

Figure 5: The radial velocity profiles along the z-axis at r=0.5L with different aspect ratios: H1/L=0.175, H1/L=0.275, H1/L=0.375, H1/L=0.475, and H1/L=0.575.

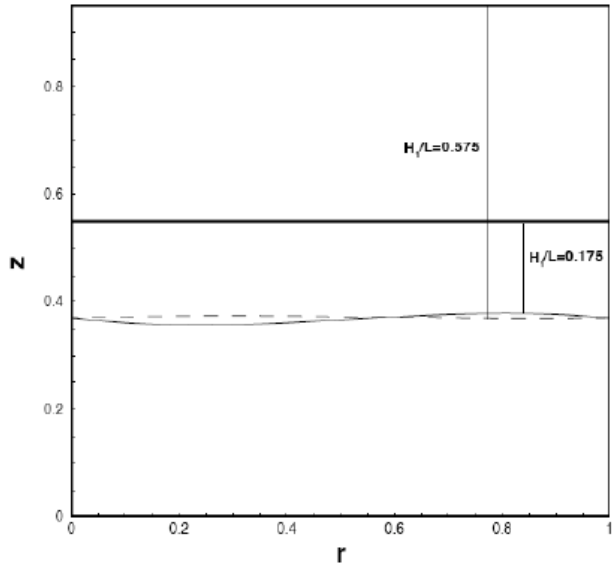

Figure 6: The interface deformation with two different aspect ratios: H1/L=0.175, and H1/L=0.575.

In the last, we examine the effect of the Ca number on the interface deformation. With $\rho_1=\rho_2=1.0$, $v_1=10v_2$, $c_{p1}=c_{p2}=1.0$, $\sigma_T=-1\times10^{-4}$, and $\Delta T=20$, The different Ca numbers are achieved by varying the σ_0. Figure **7** clearly exhibits that the interface deformation becomes more obvious at larger Ca. The corresponding radial velocity profiles along the z-axis at r=L are shown in Figure **8**. The intensity of the thermocapillary flow in the upper layer liquid is only slightly changed for different Ca numbers. In contrast, the intensity of the thermocapillary flow in the lower layer liquid is enhanced with increasing Ca.

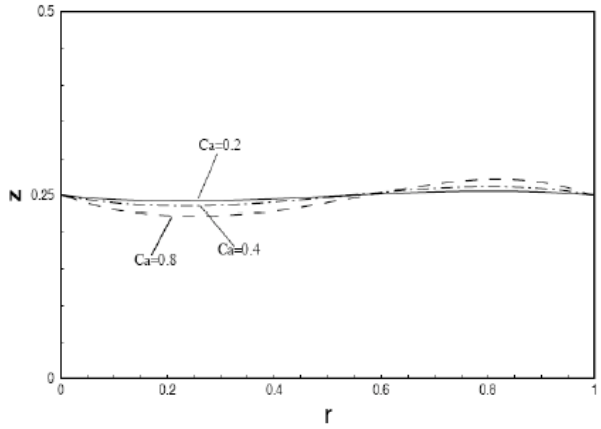

Figure 7: The interface deformation for different Ca numbers: Ca=0.2, Ca=0.4, and Ca=0.8, with v1/v2=10.

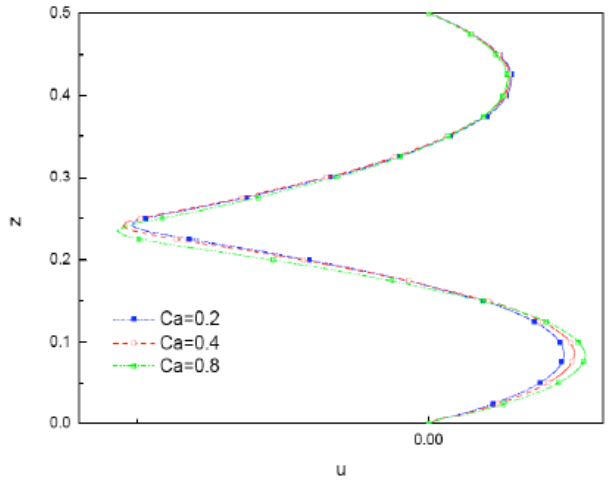

Figure 8: The radial velocity profiles along the z-axis at r=0.5L with different Ca numbers.

CONCLUSION

A numerical study on thermocapillary flow within a differentially heated annular cavity containing two-layer liquids in the absence of gravity is carried out by using the hybrid lattice Boltzmann model, which combines MRT LBM and FDM. The results indicate that, while the density in lower layer is fixed, the flow intensities in both the lower and upper liquid layers are reduced with increasing the ratio of density and the interface deformation also related to the density ratio. In addition, the effect of Capillary number on the interface

deformation is investigated, and the results show that the interface deformation becomes more obvious at larger Ca number.

ACKNOWLEDGEMENT

This work is supported by the Fundamental Research Funds for the Central Universities (No. CDJZR13248801), Program for Changjiang Scholars and Innovative Research Team in University (No. IRT13043) and Research Fund for the Doctoral Program of Higher Education of China (No. 20110191110037). Y. Kawazoe thanks the Russian Mega grant Project (No.14.B25.31.0030) “New energy technologies and energy carriers” for supporting the present research.

NOMENCLATURE

f_α	Density distribution function
f^{eq}	Equilibrium distribution function
m_α	Moment
m^{eq}	Equilibrium moment
e_α	Discrete particle speeds
c_p	Heat capacity
u	Velocities
p	Pressure
T	Temperature
n	Interface normal
k	Interface curvature
Re	Reynolds number
Ma	Marangoni number
Ca	Capillary number

Greeks

σ	Surface tension
φ	Order parameter
κ	Thermal conductivity
v	Kinematic viscosity
ρ	Density

Subscripts/Superscripts

α	Discrete speed directions (α=0,…,8)
eq	Equilibrium

REFERENCE

[1] Ostrach S. Low gravity fluid flows. Ann Rev Fluid Mech 1982; 14: 313-345. http://dx.doi.org/10.1146/annurev.fl.14.010182.001525

[2] Morton JL, Ma N, Bliss DF, Bryant GG. Magnetic field effects during liquid-encapsulated Czochralski growth of doped photonic semiconductor crystals. J Crystal Growth 2003; 250: 174-182. http://dx.doi.org/10.1016/S0022-0248(02)02261-3

[3] Cha SS, Ramachandran N, Worek WM. Heat transfer of thermocapillary convection in a two-layered fluid system under the influence of magnetic field. Acta Astronautica 2009; 64: 1066-1079. http://dx.doi.org/10.1016/j.actaastro.2009.01.018

[4] Doi T, Koster JN. Thermocapillary convection in two immiscible liquid layers with free-surface. Phys Fluids A 1993; 5: 1914-1927. http://dx.doi.org/10.1063/1.858817

[5] Liu QS, Roux B, Velarde MG. Thermocapillary convection in two-layer systems. International Int J Heat Mass Transfer 1998; 41: 1499-1511. http://dx.doi.org/10.1016/S0017-9310(97)00277-9

[6] Gupta NR, Haj-Hariri H, Borhan A. Thermocapillary flow in double-layer fluid structures: An effective single-layer model. J Colloid Interface Sci 2006; 293: 158-171. http://dx.doi.org/10.1016/j.jcis.2005.06.036

[7] Koster JN. Early mission report on the four ESA facilities: biorack; Bubble, drop and particle unit; Critical point facility and advanced protein crystallization facility flown on the IML-2 spacelab mission. ESA Microgravity News 1994; 7: 2-7.

[8] Liu H, Valocchi AJ, Zhang Y, Kang Q. Phase-field-based lattice Boltzmann finite-difference model for simulating thermocapillary flows. Phys Rev E 2013; 87: 013010. http://dx.doi.org/10.1103/PhysRevE.87.013010

[9] Penrose O, Fife PC. Thermodynamically consistent models of phase-field type for the kinetic of phase transitions. Physica D: Nonlinear Phenomena 1990; 43: 44-62. http://dx.doi.org/10.1016/0167-2789(90)90015-H

[10] Brackbill JU, Kothe DB, Zemach C. A continuum method for modeling surface tension. J Comput Phys 1992; 100: 335-354. http://dx.doi.org/10.1016/0021-9991(92)90240-Y

Received on 07-30-2015 Accepted on 08-30-2015 Published on 13-07-2016

DOI: http://dx.doi.org/10.15377/2409-5826.2016.03.01.4